


Received October 28, 2021, accepted November 26, 2021, date of publication December 6, 2021, date of current version January 7, 2022.

Digital Object Identifier 10.1109/ACCESS.2021.3133436

High-Brightness, High-Speed, and Low-Noise VCSEL Arrays for Optical Wireless Communication

ZUHAIB KHAN¹, YUNG-HAO CHANG¹, TE-LIEH PAN², YAUNG-CHENG ZHAO¹,
YEN-YU HUANG¹, CHIA-HUNG LEE³, JUI-SHENG CHANG³, CHENG-YI LIU³,
CHENG-YUAN LEE², CHAO-YI FANG², AND JIN-WEI SHI¹ ¹, (Senior Member, IEEE)

¹Department of Electrical Engineering, National Central University, Zhongli 320, Taiwan

²AboCom Systems Inc., Miaoli County 35059, Taiwan

³Department of Chemical and Materials Engineering, National Central University, Zhongli, Taoyuan City 32001, Taiwan

Corresponding author: Jin-Wei Shi (jwshi@ee.ncu.edu.tw)


This work was supported by the Ministry of Science and Technology in Taiwan under Grant 110-2622-E-008-016.

ABSTRACT The development of high-speed and high-brightness vertical-cavity surface-emitting lasers (VCSELs), which can serve as an efficient light source for optical wireless communication (OWC), play a crucial role in growth of the next generation of wireless communication networks, e.g., 6 G and satellite communications. In this work, by optimizing the size of the Zn-diffusion and oxide-relief apertures in a high-speed 850 nm VCSEL, we obtain record-high brightness ($2.9 \text{ MWcm}^{-2}\text{sr}^{-1}$ at 10 mW output) with single polarized and (quasi-) single-mode (SM) outputs under continuous wave (CW) operation. However, such high brightness output comes at the cost of spatial hole burning (SHB) effect and degraded quality of 25 Gbit/sec eye patterns. In addition, an SM VCSEL array structure is usually needed to further boost the total available optical power for long-reach OWC. Here, a novel (quasi-) SM VCSEL array structure is demonstrated which releases the trade-off between the performances of brightness and eye-pattern quality. Our demonstrated array has a special crisscross mesa connecting neighboring VCSEL units and an extra electroplated copper substrate integrated on the backside of the chip. Compared to the reference array without the copper substrate and connected active mesas, the demonstrated array exhibits a higher (quasi-) SM output power, narrower divergence angle, larger orthogonal polarization mode suppression ratio (OPSR), and flatter E-O response. This in turn leads to smaller jitter and less noise in the measured 12.5 Gbit/sec eye-patterns. The demonstrated 7×7 array exhibits a maximum SM power of around 90 mW with a $1/e^2$ divergence angle as narrow as 7° (FWHM: 5°), single polarized output (10 dB OPSR), decent relative intensity noise performance ($< -130 \text{ dB/Hz}$) and clear 12.5 Gbit/sec eye-opening. Such new device with remarkable static/dynamic performances has strong potential to further improve the product of the linking distance and data rate in the next generation of OWC channels.

INDEX TERMS Vertical cavity surface emitting lasers, semiconductor lasers, semiconductor laser arrays.

I. INTRODUCTION

High-speed and high-brightness vertical-cavity surface-emitting lasers (VCSELs) have plentiful applications nowadays. It has been suggested that such VCSEL arrays can be used as the light source in optical wireless communication (OWC) channels, one possible solution for development of the next generation of wireless communication systems for 5G, 6G and satellite communications [1], [2].

The associate editor coordinating the review of this manuscript and approving it for publication was Leo Spiekman .

A Space-Comm. network for linking different micro or nanosatellites has already been successfully established [3], [4]. A linking distance of up to hundreds of kilometers with a data transmission rate of around 20 Mbit/sec is necessary for such systems [3], [4]. A high CW power (hundreds of mW) high-brightness, high-speed light source plays a crucial role in the afore-mentioned applications. Compared with their counterparts i.e., the edge-emitting lasers (EELs), VCSELs exhibit better radiation resistance [5], [6] and, with proper heat-sinking, their output power can be scaled up along with the size of the 2-D VCSEL array [7], [8].

In order to attain high-brightness output, it is highly desirable to have a VCSEL array with a high output power and narrow divergence angle. For most of the high-power VCSELs reducing the reflectivity of the Distributed-Bragg reflector (DBR) mirror is usually preferred to boosting the output power. However, this approach will reduce the photon lifetime (τ_p) inside the VCSEL cavity, which in turn leads to a more pronounced relaxation oscillation phenomenon in the measured electrical-to-optical (E-O) frequency responses and higher relative intensity noise (RIN) from the light output of the VCSEL [9], [10] which impedes their application for communications. One of the most effective ways to achieve an output beam with a narrow far-field divergence angle is to assemble the VCSEL array from several single-mode (SM) VCSEL units [11], [12], which usually have a perfect Gaussian beam output with narrow divergence angle. Various VCSEL structures capable of producing highly SM power have been reported previously including surface-relief [13], Zn-diffusion [14], photonic crystal [15], and anti-guide (leaky) cavity structures [16]. However, the spatial hole burning (SHB) effect that arises from the high density of optical power in the high brightness output beam of these high-power SM VCSELs is accompanied by significant low-frequency roll-off in their electrical-optical (E-O) frequency responses and degradation in eye-pattern quality for high-speed data transmission [17]–[19]. Furthermore, in contrast to the MM VCSELs, the SM VCSEL usually has a smaller damping factor (γ), which results in pronounced resonances in the E-O and RIN frequency responses [20], [21]. This in turn leads to serious degradation in the eye pattern under high output power and large signal modulation. In this study, by optimizing the sizes of the Zn-diffusion and oxide-relief apertures in a high-speed 850 nm VCSEL, we obtain a record-high brightness ($2.9 \text{ MWcm}^{-2}\text{sr}^{-1}$) at a 10 mW output with a 7° FWHM (full width at half maximum) divergence angle, and single polarized and (quasi-) single-mode (SM) outputs under continuous wave (CW) operation. However, such high brightness and quasi-SM output power ($\sim 10 \text{ mW}$) come at the cost of a degradation in the quality of the 25 Gbit/sec eye patterns under large signal modulation. A novel VCSEL array structure is thus designed to further increase the maximum available optical power, while sustaining the high brightness, and improving the eye pattern quality for long-reach OWC applications. This structure can overcome the fundamental trade-offs between the brightness, RIN and eye pattern quality under large signal modulation. In contrast to the traditional VCSEL arrays in which the various independent single VCSEL cavities are connected in parallel, our new demonstrated VCSEL array has crisscross mesas connecting each VCSEL cavity [22]–[24]. In addition, an electroplating process is performed to integrate an additional copper substrate on the backside of our array. In each single VCSEL unit in the array, Zn-diffusion and oxide-relief structures are adopted to obtain the high-brightness (single-mode) output and relax the RC-limited bandwidth [25], [26]. This array

exhibits improvements in performance in terms of a higher (quasi-) SM output power, narrower divergence angle, lower RIN, and better quality of eye-opening for high-speed data transmission when compared to its traditional counterparts without connections between neighboring active mesas or the copper substrate. The improvements in static/dynamic performances are due to the dilution of the photon density in the SM output pattern from each VCSEL unit produced by the extended mesas along with the VCSEL cavity. Moreover, the external strain induced by the electroplated copper substrate leads to a single polarized lasing mode and an increase of the fundamental mode selectivity, which respectively reduces the RIN peak and further enhances the brightness of the output beam [27]–[29]. The demonstrated 7×7 array exhibits a maximum SM power of around 91 mW with a $1/e^2$ divergence angle as narrow as 7° (FWHM: 5°), single polarized output (10 dB orthogonal polarization suppression ratio), and clear eye-opening under 12.5 Gbit/sec modulation. This novel high-speed, high-brightness and low RIN ($< -130 \text{ dB/Hz}$ from dc to 20 GHz) 850 nm VCSEL array opens up new possibilities for the next generation of free-space optical communication.

II. DEVICE STRUCTURE AND FABRICATION

Figure 1 (a) shows top views of the demonstrated 7×7 VCSEL array. Here, we fabricated two kinds of VCSEL array structure of each size for comparison: in one kind each VCSEL unit is connected by crisscross mesas (array A); the other uses the traditional VCSEL array structure without connections between each mesa (array B). Here, the crisscross mesas in array A may be treated as optical waveguides that connect different active VCSEL units [22], [24] and are highlighted in these two pictures. Figure 1 (b) shows conceptual cross-sectional views of the active light-emitting mesa and passive waveguides in array A. Zn-diffusion and oxide-relief processes have been performed on each of the active VCSEL units aimed at manipulating the optical transverse modes and relaxing the RC-limited bandwidth of the array [25], [26], respectively. The passive waveguides between the different active mesas are composed of an epi-layer structure in the VCSEL cavity [22], [23]. The p- and n-type distributed Bragg reflectors (DBRs) act as waveguide claddings while the active layers acts as the waveguide core. The passive waveguide regions are sealed by a dielectric film to isolate them from the external current injection. The optical confinement in the transverse direction is enhanced by the application of Zn-diffusion apertures in the passive waveguide regions. The detailed geometry and size of the diffusion depth and width are specified in Figures 1 (a) and (b). For our cavity design, the photoluminescence (PL) peak wavelength of our MQW active region is at around 838 nm at RT. Based on the measured Bragg wavelength ($\sim 853 \text{ nm}$) of the VCSEL cavity, the corresponding cavity-to-PL detuning wavelength is around 15 nm. Such a design can not only improve the high-temperature performance of the VCSEL [26] but

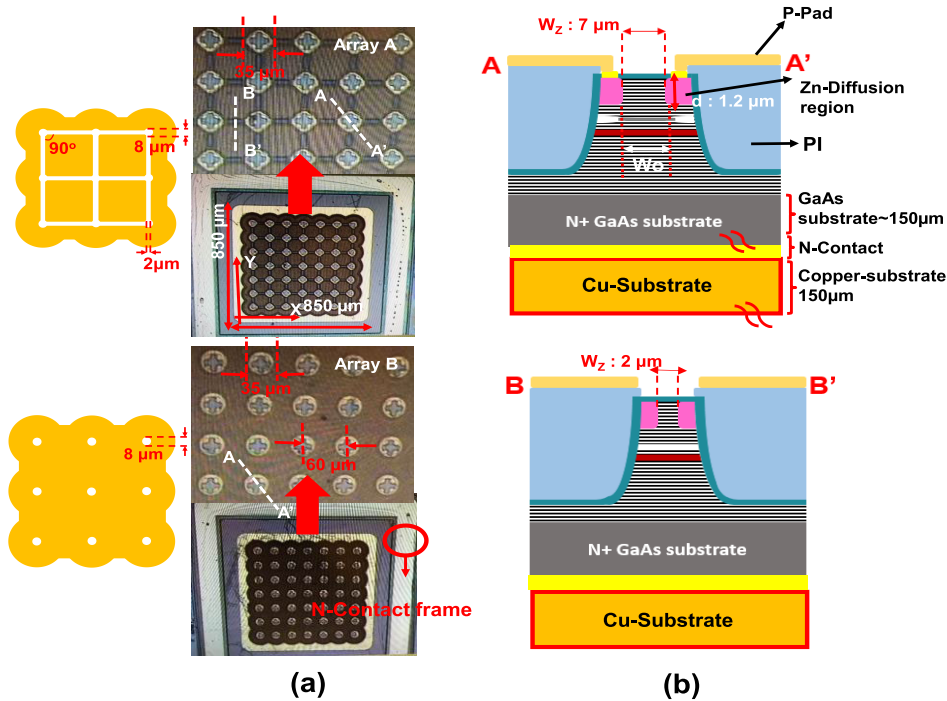


FIGURE 1. (a) Top view of the demonstrated 7×7 VCSEL array (A and B). (b) Conceptual cross-sectional view of the active mesa and passive waveguides in array A. The inset in (a) shows the layout of our Zn-diffusion apertures.

also ensure the transparency of our passive waveguide for the propagation of lasing light with a central wavelength at around 850 nm. Optical confinement in the direction perpendicular to the wafer surface of the passive waveguide is achieved by the index contrast between the III-V active multiple quantum wells (MQWs) and the thin (~ 25 nm) air layer, which is realized by the oxide-relief process, as discussed above. The lossy Zn-diffusion regions in the junction between the waveguides and the active mesas have been removed, which changes the Zn-diffusion apertures from ring- to fan-shaped, as shown in the insets of Figure 1 (a). Here, the mask defined Zn-diffusion aperture size is at $8 \mu\text{m}$. Due to lateral diffusion, the finalized W_z of fabricated device is at around $7 \mu\text{m}$, as specified in Figure 1 (b). This thus enhances the mutual coupling between the different VCSEL units through the connections through optical waveguides in array A. For details about the design and simulation of our passive waveguide the interested reader can refer to our previous work [24]. Here, we used the commercially available Lumerical¹ software to simulate the optical waveguide structure. The simulation result indicates that the different light emission units in the array cannot be effectively linked due to the large propagation loss ($1 \text{ dB}/\mu\text{m}$). Although the coherence between the different emitters cannot be enhanced through a waveguide connection, the simulated optical field distribution suggests that there is still an optical

power penetration depth of around $8 \mu\text{m}$ ($1/e^2$; -8 dB) into the waveguide. This can increase the effective size of the optical cavity of each emitter unit and greatly changes the static and dynamic performance of the array, as will be discussed in greater detail later. There are three key parameters for the active mesa which determine the mode characteristics of the single device: W_z , W_o , and d . Here, W_z and W_o represent the diameter of the Zn-diffusion aperture and oxide-confined aperture, respectively, and d is the Zn-diffusion depth. The addition of Zn-diffusion apertures in the top p-type DBR layers of our VCSEL will induce extra loss in the peripheral region of the optical aperture. Higher order mode lasing can thus be suppressed in the Zn-diffused DBR region due to free-carrier absorption and reduction in reflectivity caused by the disordering [14], [17]. The disordering of the DBR layers allows us not only to manipulate the number of optical transverse modes inside the VCSEL cavity, as discussed elsewhere, but can also reduce the differential resistance of the VCSEL [14], [17]. By properly optimizing the relative sizes of these three parameters to allow significant Zn-diffusion induced internal loss (α_i) in the current-confined (gain) region, the device demonstrates high single-mode (SM) performance under the full range of bias currents [11], [15], [18]. The values of W_z and d for all VCSEL units in arrays A and B are fixed at 7 and $1.2 \mu\text{m}$, respectively. Different values of W_o are adopted to study the influence of the output optical spectra of the VCSEL units on the static and dynamic performance of both arrays (A and B). The epi-layer structure which

¹Lumerical, an Ansys Company, Suite 1700, 1095 West Pender Street V6E 2M6 CA BC Vancouver, Canada.

is grown in a molecular beam epitaxy (MBE) chamber (Intelligent Epitaxy Technology Inc.)² is composed of five compressive strained $\text{In}_{0.1}\text{Ga}_{0.9}\text{As}/\text{Al}_{0.35}\text{Ga}_{0.65}\text{As}$ MQWs sandwiched between 39-paired n-type and 20-paired p-type $\text{Al}_{0.93}\text{Ga}_{0.07}\text{As}/\text{Al}_{0.15}\text{Ga}_{0.85}\text{As}$ Distributed-Bragg-Reflector (DBR) layers with a dual $\text{Al}_{0.98}\text{Ga}_{0.02}\text{As}$ layer (25 nm thickness) for oxidation. The fabrication of the array starts with the Zn-diffusion process. The application of a high-quality Si_3N_4 film is necessary to serve as a mask for the high-temperature diffusion process. The mask defined diameter of the optical aperture (without Zn-diffusion) is around 8 μm . Considering lateral Zn-diffusion, the final W_z after completion of the Zn-diffusion process is around 7 μm and $\sim 1.2 \mu\text{m}$ in depth (d), as discussed in Figure 1. After the diffusion process, crisscross mesas etching is performed. Although the shape of the mesa is not circular after wet etching a circular current-confined area can still be obtained after the wet oxidation process. In order to obtain different sizes of W_o , 2 different diameters of mesas are used, resulting in W_o of 11 and 14 μm . After p-type contact metallization (Ti/Au;50/200 nm), the device is passivated by the application of a SiO_2 layer (~ 150 nm). An $\sim 3 \mu\text{m}$ thick polymethylglutarimide (PI) layer is then deposited for planarization. Finally, an $\sim 2 \mu\text{m}$ thick Ti/Au layer is evaporated onto the topside of the chip to form metal pads for on-wafer probing. As shown in Figure 1, an electroplating process is performed onto n-metal contacts on the backside of the fabricated chips, which have 150 μm thick n^+GaAs substrates (after lapping). The copper substrate is grown to around 100 μm in thickness. The strain induced by the composite substrates (GaAs and copper) has a significant influence on the dynamic and static performance of VCSEL devices, which will be discussed in detail later.

III. MEASUREMENT RESULTS

Firstly, we investigate a single reference VCSEL with optimized values of W_z , W_o , and d for highest brightness performance. Figure 2 shows the measured L-I-V curves and bias dependent output spectra of such device. Here, the chosen values of W_z , W_o , and d are 6, 9, and 1.6 μm , respectively. The electroplated copper substrate is not applied to this single reference device. As can be seen, the (quasi-) SM output remains stable from near the threshold until saturation occurs with the maximum output power at around 10 mW and a side-mode suppression ratio (SMSR) of 12 dB. Figure 3 (a) shows the measured 2-D and corresponding 1-D far-field patterns of this device. We can clearly see that a single-spot and Gaussian-like far-field distribution can be sustained under the full range of bias currents with a divergence angle as narrow as FWHM: 7° under the saturation bias current (15 mA). By assuming the far-field distribution of the device to be cone-shaped with a point angle of 7° , we can then determine the corresponding steradian

and the brightness of our output beam [30]. Here, the area of the light emission aperture (S) is determined by W_z . The brightness can be as high as $2.9 \text{ MWcm}^{-2}\text{sr}^{-1}$ the highest brightness ever reported in the electrical pumping SM VCSELs, including for an 850 nm VCSEL with a linear grating [31] ($1.7 \text{ MWcm}^{-2}\text{sr}^{-1}$ at a 6.5 mW output with a 9° divergence angle) and long-wavelength VCSEL [19] with buried tunnel junctions ($1.36 \text{ MWcm}^{-2}\text{sr}^{-1}$ at an 8 mW output with a 8° divergence angle). The single-polarized output from the VCSEL is also an important feature for the process of light coupling into different components [31]. The polarization states of most of the reported VCSELs hop between two orthogonal orientations ($\langle 011 \rangle$ and $\langle 01\bar{1} \rangle$) with a change of bias current [28], [29]. Here, we define the measured optical power ratio in these two orientations ($\langle 01\bar{1} \rangle / \langle 011 \rangle$) as the orthogonal polarization mode suppression ratio (OPSR), which can be obtained by using a polarizer during L-I curve measurement. Figure 3 (b) shows the measured bias dependent OPSR, which can be as high as around 20 dB over a wide range of bias currents. This OPSR performance is comparable with that of the 850 nm VCSEL integrated with a linear grating on the top DBR mirror [31]. However, as discussed above, the cost of such high brightness output is the SHB induced low-frequency roll-off in its E-O response and the significant degradation in the eye pattern quality under large signal modulation [17], [18]. Figures 4 (a) and (b) show the bias-dependent E-O responses and 25 Gbit/sec eye patterns of the demonstrated device measured under two different bias currents (9 and 12 mA). As can be seen, there is an over 6 dB roll-off in the low-frequency (< 5 GHz) part of E-O response, which leads to a large jitter in the measured eye-patterns. In order to overcome the above problems in high brightness VCSELs for high-speed OWC and further increase the maximum available optical power, a novel high brightness VCSEL array structure, as shown in Figure 1, is designed which will be investigated in the following parts of the paper. A detailed comparison was made between the performance of both array structures (A and B) for the cases with and without the extra electroplated copper substrate. We first compared the performance of devices without the copper substrate. Figures 5 (a) and (b) show the measured detailed L-I-V curves for arrays A and B having different sizes of W_o (14 and 11 μm), under room temperature (RT) operation. The insets show the measurement results for the corresponding single reference device. As can be seen, in array A, with waveguide connections between the different VCSEL units, the measured I_{th} is linearly proportional to the number of VCSEL units (i.e., 49). This result implies that the injected current, which spreads from the active mesa to the passive waveguide region, is negligible. The significant increase of I_{th} with W_o can be attributed to the increase of the Zn-diffusion induced intra-cavity loss when the size of W_o becomes larger than the size of the Zn-diffusion aperture (W_z) [17]. The payoff for the higher I_{th} in our array is the high single-mode (SM) output [17]. In addition, we can clearly see that the

²Intelligent Epitaxy Technology, Inc. 1250 E Collins Blvd, Richardson, TX 75081, USA.

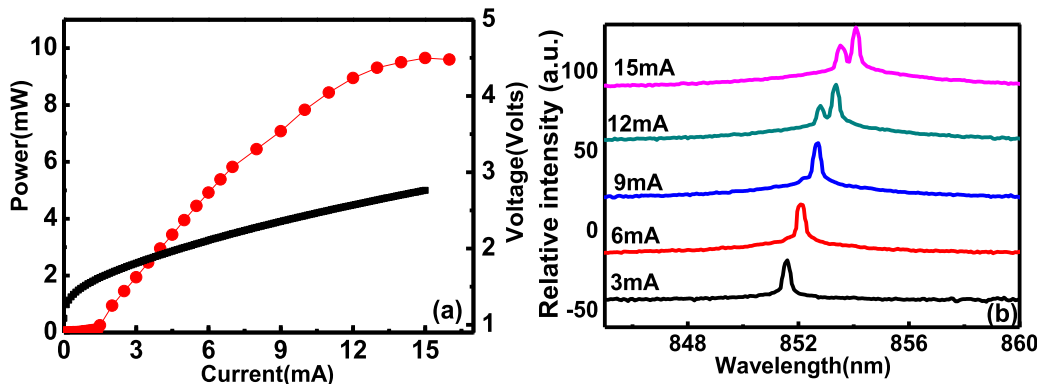


FIGURE 2. Measured (a) L-I-V curves and (b) bias dependent optical spectra of high-brightness single VCSEL unit.

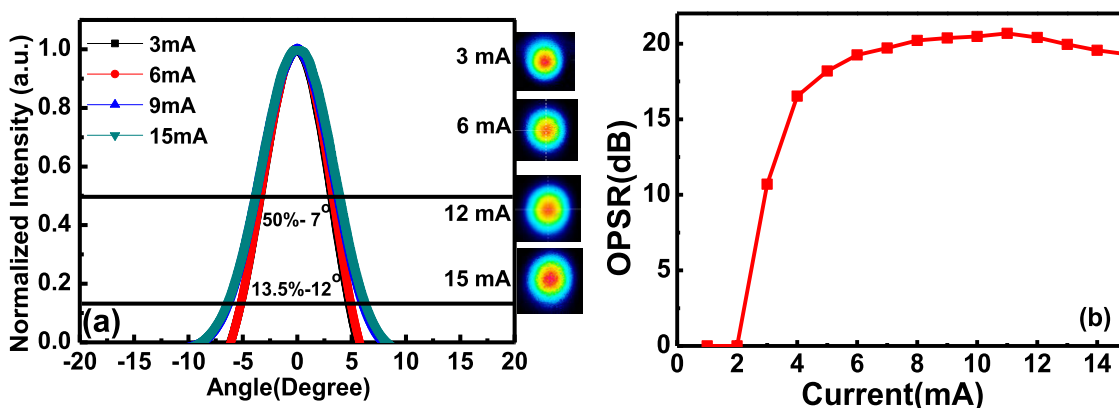


FIGURE 3. (a) Measured 1-D and 2-D far-field patterns and (b) bias dependent OPR of high-brightness single VCSEL unit.

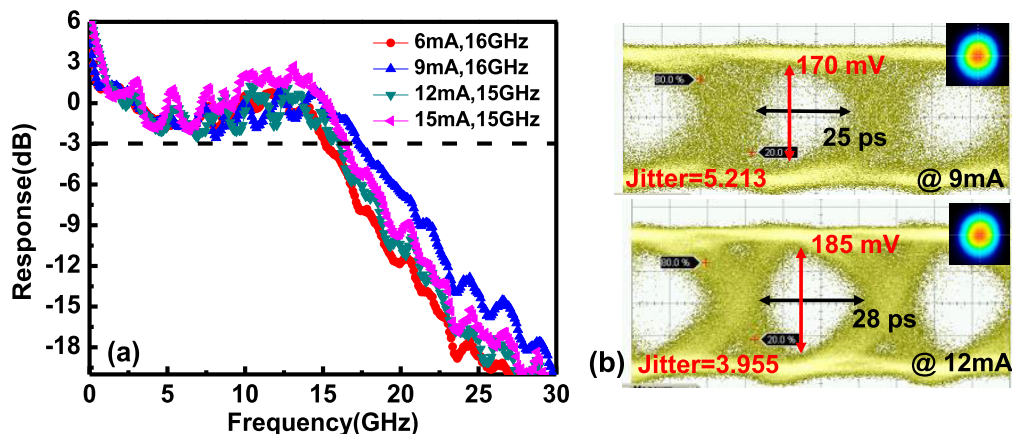


FIGURE 4. (a) Measured bias-dependent E-O frequency response and (b) measured 25 Gbit/sec eye pattern of high-brightness single VCSEL unit.

maximum output power of array A is significantly higher than that of array B (100 vs. 110 mW under a 500 mA bias current) for the larger oxide aperture (W_o : 14 μm) with quasi-SM performance. The measured bias dependent output optical spectra of arrays A with two differently sized W_o (11 and 14 μm) and array B with a 11 μm W_o is shown in

Figures 6 to 8, respectively. We can clearly see that arrays A and B can keep a quasi-single-mode (QSM) or single-mode (SM) output under the entire range of bias currents. The difference in behavior in the optical spectra performance between array A and array B with the same W_o is because the extended optical waveguides (crisscross mesa) in array A will

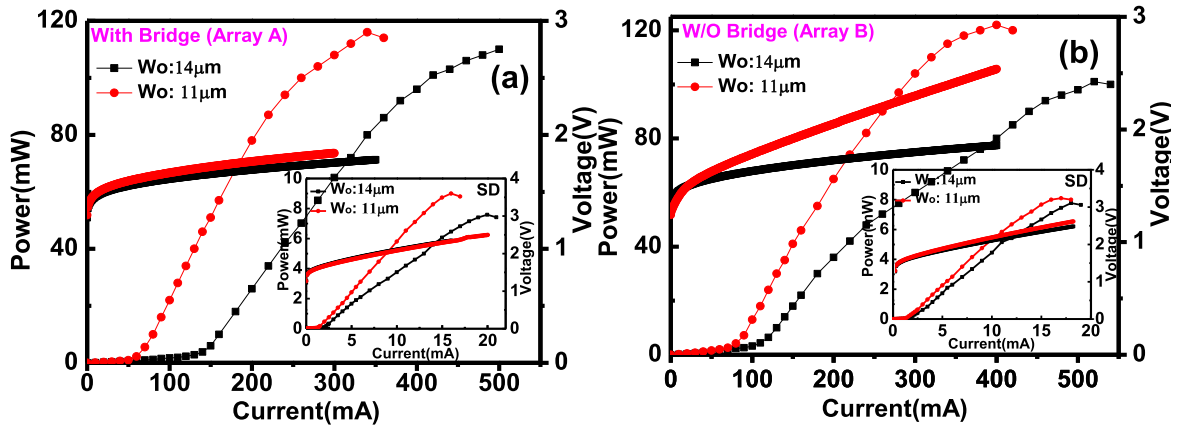


FIGURE 5. (a) Measured L-I-V curves of VCSEL array A having different oxide aperture (W_0 : 14 μm , 11 μm) and reference single unit (inset) (b) Measured L-I-V curves of VCSEL array B having different oxide aperture (W_0 : 14 μm , 11 μm) and reference single unit (inset).

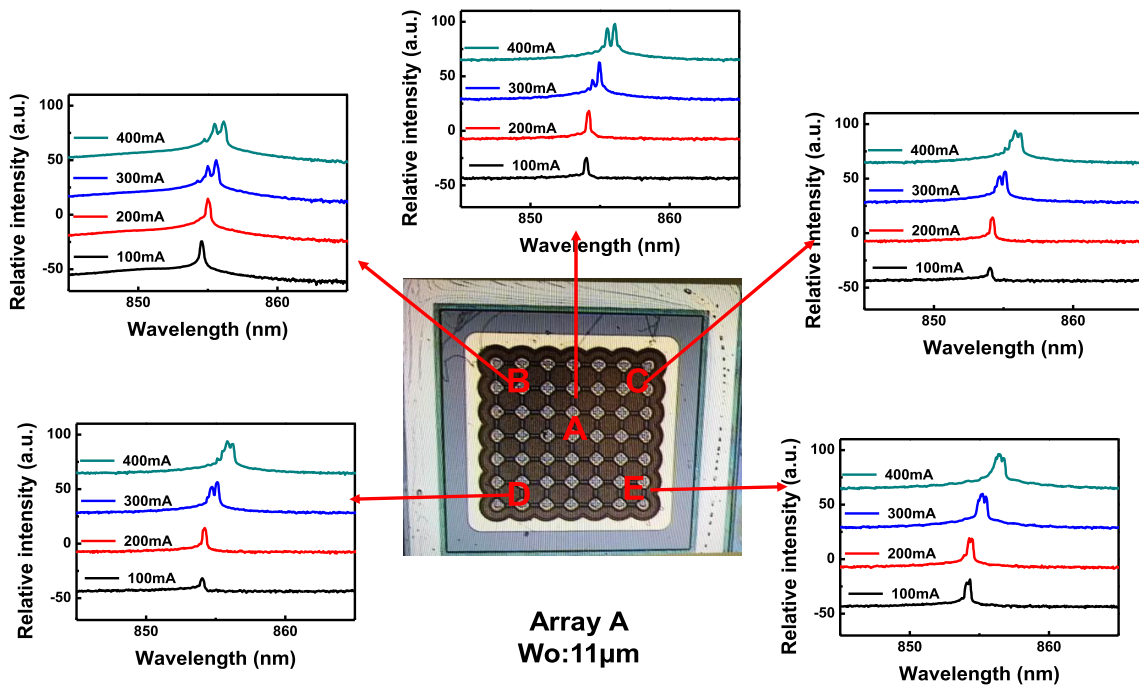


FIGURE 6. Measured bias dependent optical spectra of array A with W_0 : 11 μm at different locations on the array under continuous wave (CW) operation.

enlarge the size of the optical cavity and induce additional optical transverse modes. Figure 9 shows the measured one-dimensional (1-D) (in the x-direction) and 2-D far-field patterns (FFPs) of arrays A and B under different bias currents at continuous wave (CW) operation. A charge-coupled device (CCD) camera was installed just above the array to take pictures of the far-field patterns for 2-D measurement.

Neutral density (ND) filters were inserted between the array and the CCD in order to avoid saturation of the camera and the influence of optical feedback on the measured patterns. The 1-D patterns were constructed from the measured data points in our 2-D patterns. We can clearly see

that Gaussian like far-field patterns (FFP) can be sustained for both arrays with different oxide apertures (W_0 : 14 μm , 11 μm) regardless of the bias current. Furthermore, when the W_0 reaches 14 μm the FFPs of both show significant narrowing. This can be attributed to the increase of Zn-diffused intra-cavity loss in the case of the larger W_0 , which in turn leads toward the highly single-mode performance and the narrowing of the far-field divergence angle [17]. In addition, array A with the same W_0 of 14 μm as array B exhibits a smaller divergence angle ($1/e^2$: $\sim 8^\circ$ vs. $\sim 11^\circ$) under a 400 mA CW operation current. These FFP and L-I-V measurement results indicate that when the VCSEL array

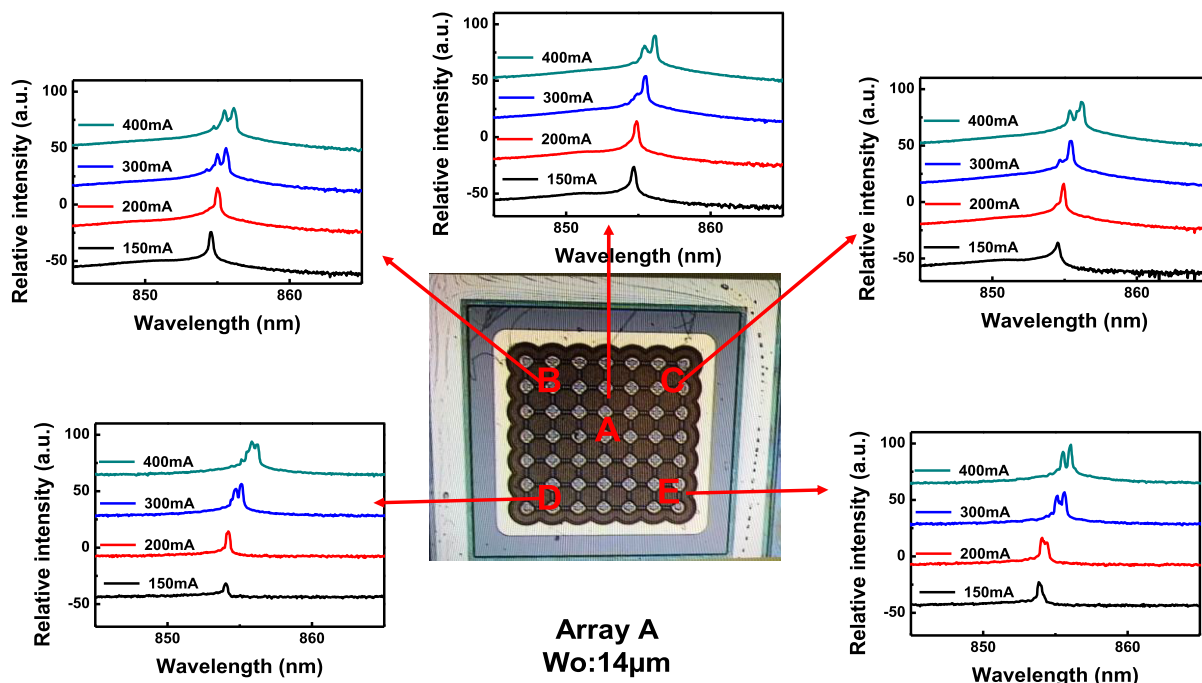


FIGURE 7. Measured bias dependent optical spectra of array A with W_0 : $14 \mu\text{m}$ at different locations on the array under continuous wave (CW) operation.

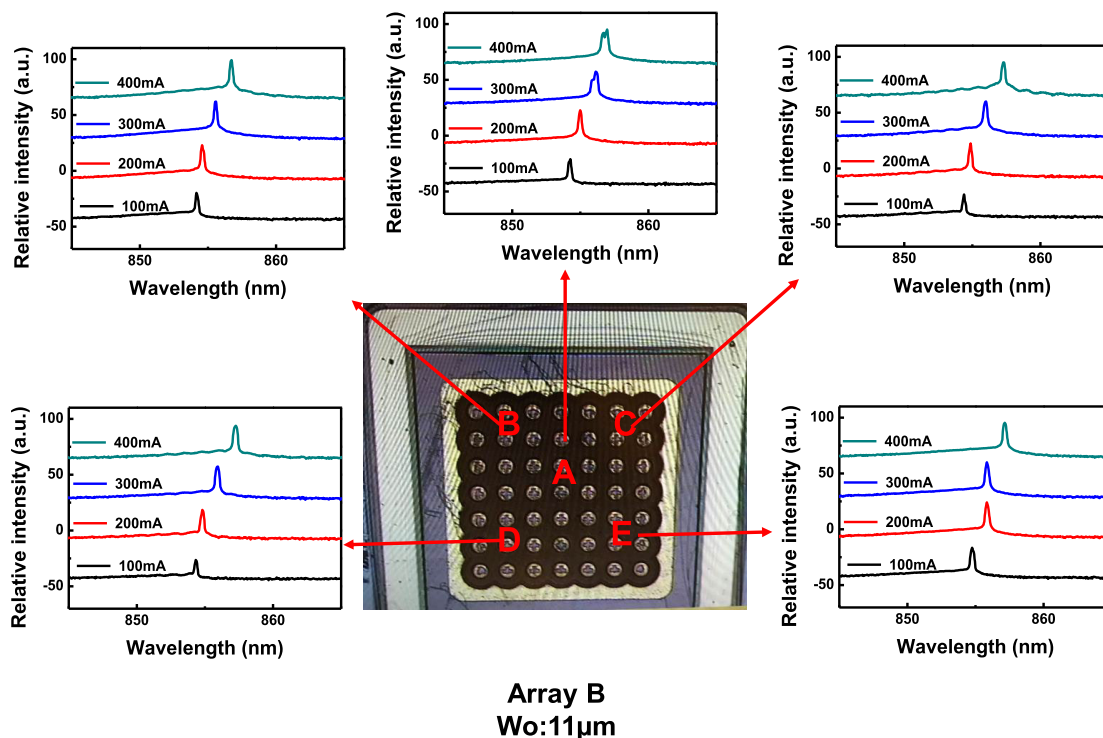


FIGURE 8. Measured bias dependent optical spectra of array B with W_0 : $11 \mu\text{m}$ at different locations on the array under continuous wave (CW) operation.

output varies from quasi-SM to SM with an increase in the W_0 , the increase in the Zn-diffused intra-cavity loss will lead to degradation in the wall plug efficiency (WPE)

performance. The demonstrated crisscross mesa structures in array A can effectively dilute the photon density, resulting in an enhancement of the WPE (output power) and sustainment

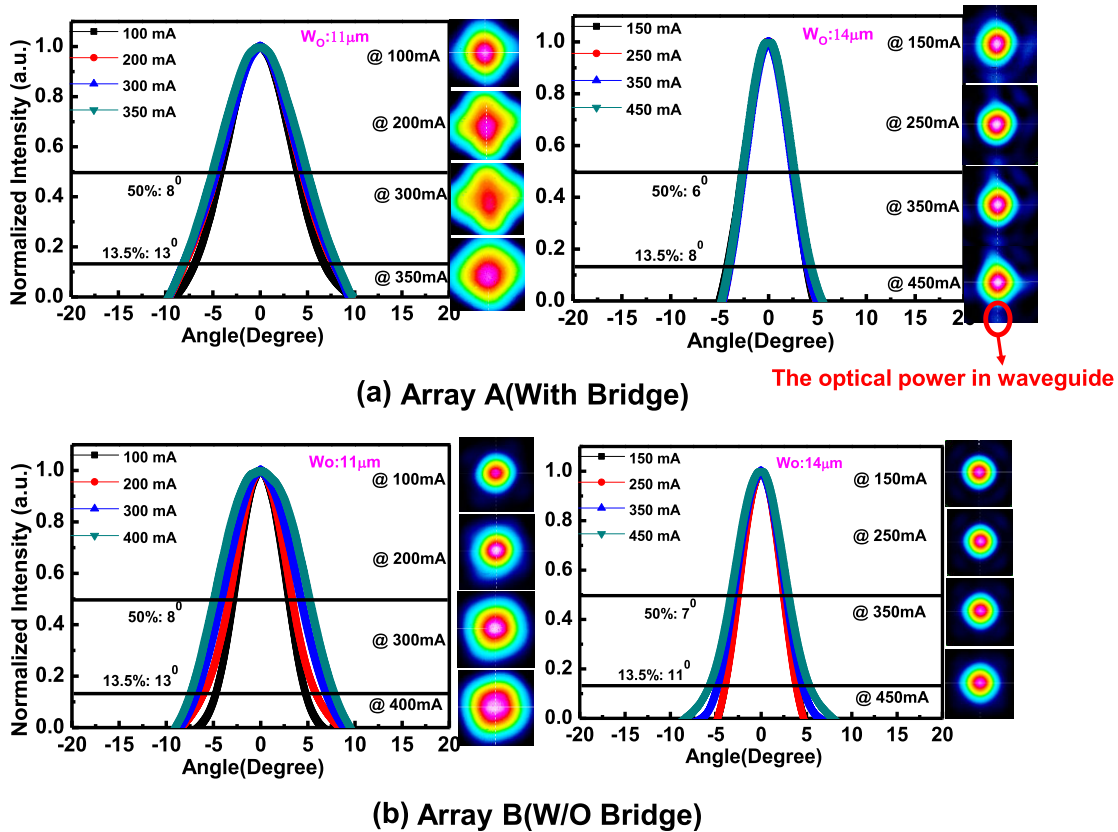


FIGURE 9. Measured 1-D and 2-D far-field patterns of (a) array A and (b) array B having two sizes of W_0 ($11 \mu\text{m}$, $14 \mu\text{m}$) under different CW bias currents and prior to electroplating the copper substrate.

of the single-spot FFP with even a narrower divergence angle and higher brightness. The improvement in brightness of array A can be attributed to the increase in the effective optical emission area without inducing higher-order modes. As specified in the insets of Figure 9 for the measured 2-D FFPs of array A, we can clearly see that light leakage through the four passive waveguides can be treated as an increase of the effective optical volume in the near field and lead to narrowing in its far-field pattern. This measurement result is consistent with our optical simulation result. Nevertheless, the Zn-diffusion induced intra-cavity loss must be properly adjusted, as determined by the relative sizes of the W_0 and W_z [17] to suppress the generation of higher-order transverse modes when the optical volume is increased. Taking the measured FFPs of array A with W_0 as $11 \mu\text{m}$ as an example, we can clearly see that they have become significantly deformed from circular to rhombic in shape due to the extended passive waveguides around the active cavity and the smaller intra-cavity loss as compared to that of array A with a W_0 of $14 \mu\text{m}$. The high-speed electrical-to-optical (E-O) performance of the fabricated arrays was measured by a lightwave component analyzer (LCA), composed of a network analyzer (Anritsu 37397C) and a calibrated photoreceiver module (VI Systems: D50-1300 M)³, which could cover an optical window from

wavelengths of 850 to 1310 nm. Figures 10 (a) to (c) show the measured bias dependent E-O frequency responses of a single reference VCSEL unit, array A and array B, respectively, for different oxide aperture sizes (W_0 : $11 \mu\text{m}$, $14 \mu\text{m}$). Thanks to the Zn-diffusion and oxide-relief processes, which can effectively release the RC-limited bandwidth of the VCSEL array [25], [26], the measured 3-dB E-O bandwidth of array A with a W_0 of $14 \mu\text{m}$ is quite close to that of the single reference VCSEL (~ 11 vs. 12 GHz) under the same average bias current (~ 8 mA). Moreover, we can clearly see that, in contrast to array B, which has a low-frequency roll-off of around 4 dB due to the spatial hole burning (SHB) effect [17]–[19] this roll-off has been completely eliminated in the measured E-O responses of array A. From the static and dynamic measurement results, we can conclude that the extended passive waveguide structure used in array A can not only provide an FFP with a narrower divergence angle (higher brightness) than that of the traditional SM array but also an improvement in the E-O frequency response due to the diluted photon density inside the VCSEL cavity. On the other hand, in the cases where W_0 is $11 \mu\text{m}$, the single reference device exhibits a faster speed performance than does array A under the same averaged bias current (6 mA; 17 vs. 14 GHz). This phenomenon can be attributed to the VCSEL output switching from highly SM (W_0 : $14 \mu\text{m}$) to quasi-SM or MM (W_0 : $11 \mu\text{m}$), the SHB effect is no longer the speed bottleneck and device heating becomes the major bandwidth

³VI Systems GmbH, Hardenbergstrasse 7, 10623 Berlin, Germany.

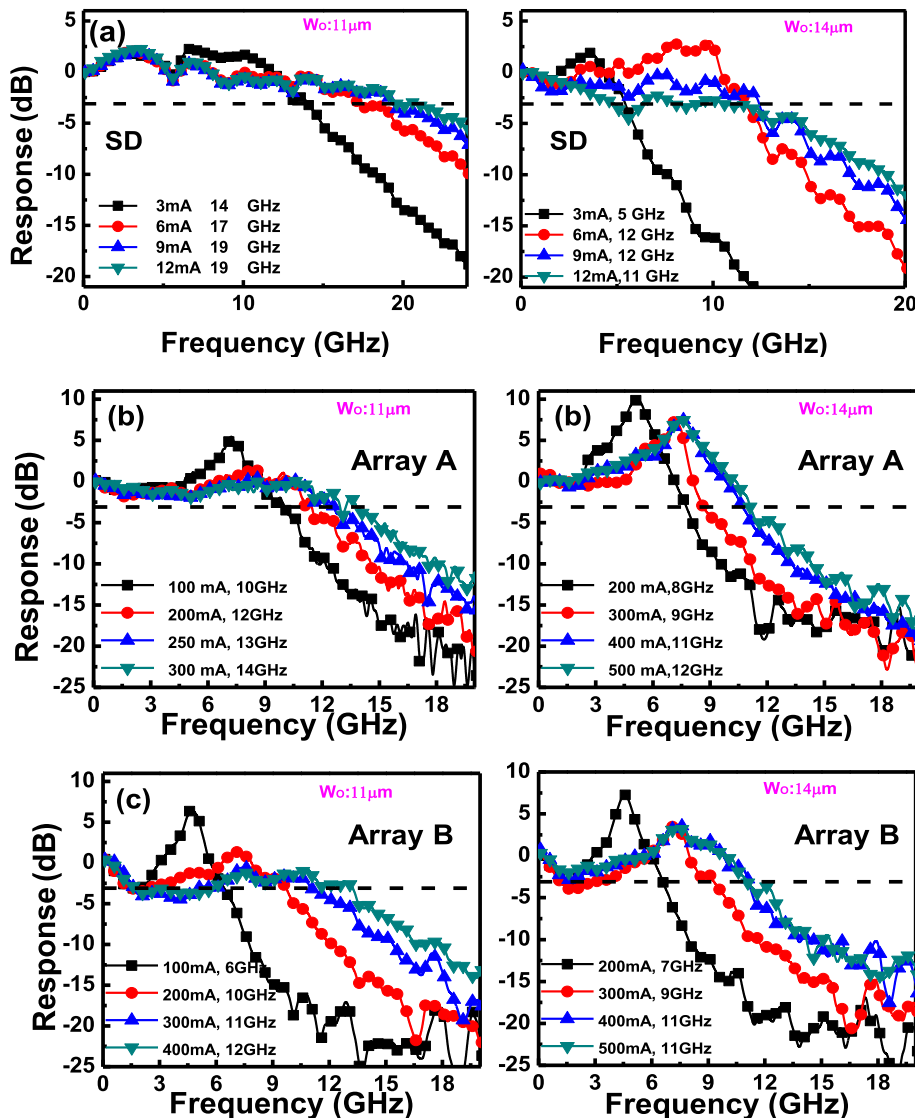


FIGURE 10. (a) Measured bias dependent E-O frequency response of (a) single reference VCSEL unit, (b) array A, and (c) array B with W_0 of $11 \mu\text{m}$ and $14 \mu\text{m}$.

limitation factor in array A. Higher speed with quasi-SM and MM performance ($W_0: 11 \mu\text{m}$) can be expected of array A by further improving the thermal management in our device [32]. In addition, we can clearly see that for both array structures A and B, when their output optical spectra switches from MM ($W_0: 11 \mu\text{m}$) to SM ($W_0: 14 \mu\text{m}$), it is hard to minimize the relaxation oscillation peak in the E-O responses with the increase of bias current [20], [21]. Such a phenomenon can be attributed to the fact that the SM VCSEL usually has a smaller damping factor (γ) than that of the MM counterpart [21]. This accompanies a large resonant peak of RIN [20] and significant degradation in eye pattern quality. The minor SHB effect induced by the electroplated copper substrate, which will be discussed later, pulls down the significant resonance in the E-O (RIN) response with a small ($<2 \text{ dB}$) low-frequency roll-off, lowers the RIN peak, and improves

the overall large-signal modulation performance. The static and dynamic performance of the array after performing the electroplating process is discussed in detail below. Figure 11 compares the L-I-V curves of array A before and after the electroplating of the copper substrate. As can be seen, there is some degradation in the maximum output power and the I_{th} after electroplating. This can be attributed to the more pronounced SHB effect which occurs in the electroplated VCSEL, which has highly SM performance with narrower far-field divergence angles. Figures 12 (a) and (b) show the 1-D/2-D FFPs of arrays A and B, respectively, measured after integration of the copper substrate. In contrast to the FFPs measured before electroplating, as shown in Figure 9, both arrays show further narrowing of the FFPs when the W_0 is equal to $14 \mu\text{m}$. Figures 13 shows the corresponding optical spectra for array A with W_0 of $14 \mu\text{m}$ measured under

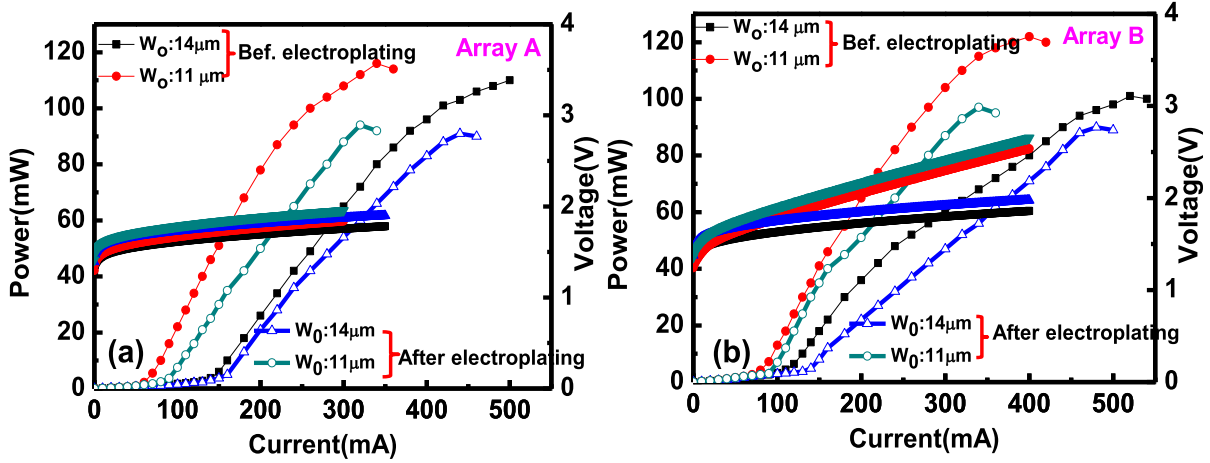


FIGURE 11. Measured L-I-V curves of (a) array A and (b) array B with two different sizes of W_0 ($11 \mu\text{m}$, $14 \mu\text{m}$) before and after electroplating of the copper substrate.

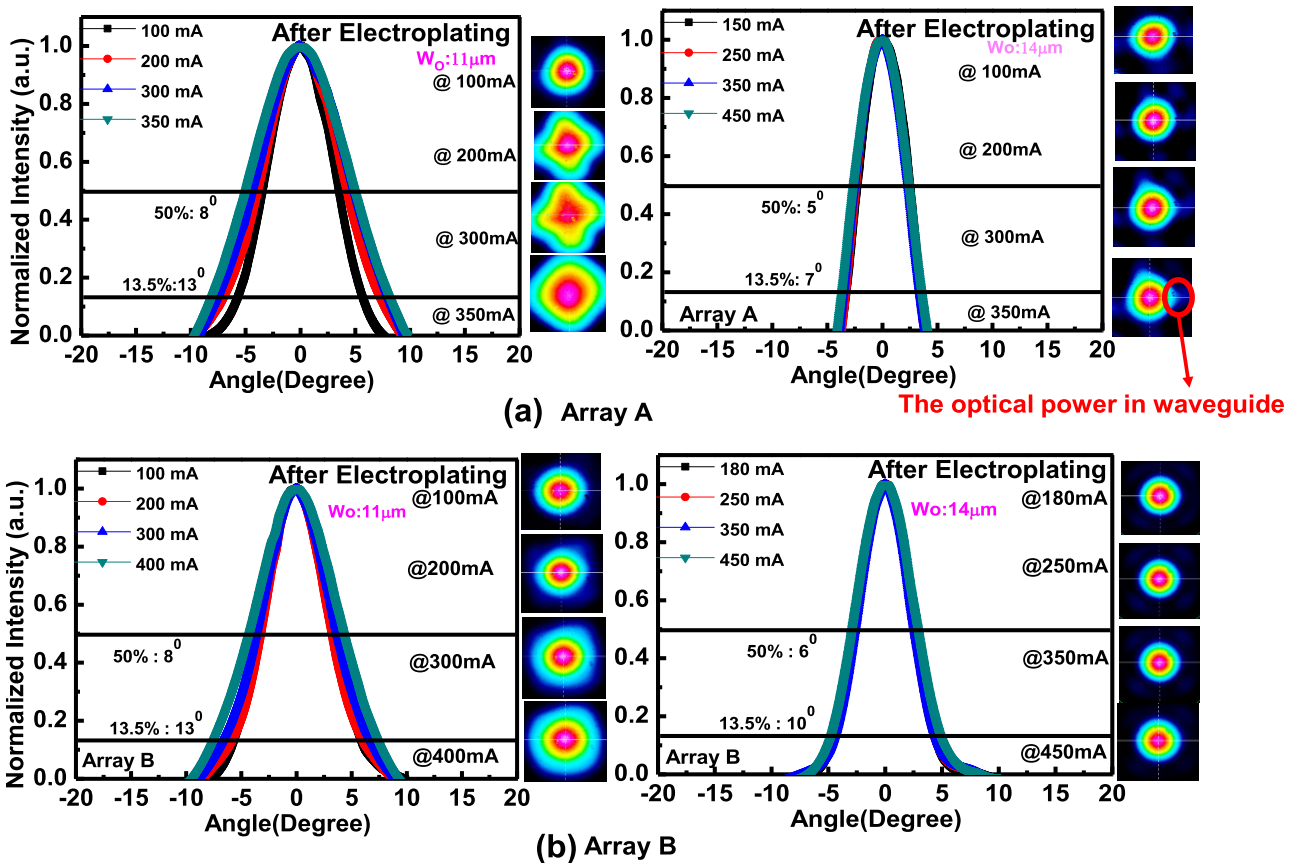


FIGURE 12. Measured 1-D and 2-D far-field patterns of (a) array A and (b) array B having two sizes of W_0 ($11 \mu\text{m}$, $14 \mu\text{m}$) under different CW bias currents, after electroplating of the copper substrate.

different bias currents. We can clearly see that compared with the quasi-SM optical spectra appearing in Figures 6 and 7, the optical spectra for array A with a W_0 of $14 \mu\text{m}$ show a switch from quasi-SM to SM after performing electroplating. The enhancement in fundamental mode selectivity of our VCSEL structure can be attributed to the single polarized

lasing mode induced by the strain caused by the addition of the electroplated copper substrate [27]. As compared to array A with the $14 \mu\text{m}$ W_0 , the electroplated copper substrate induced mode switching is less pronounced for the case of $11 \mu\text{m}$ W_0 . This is because the device with that size of W_0 has a nearly multi-mode performance

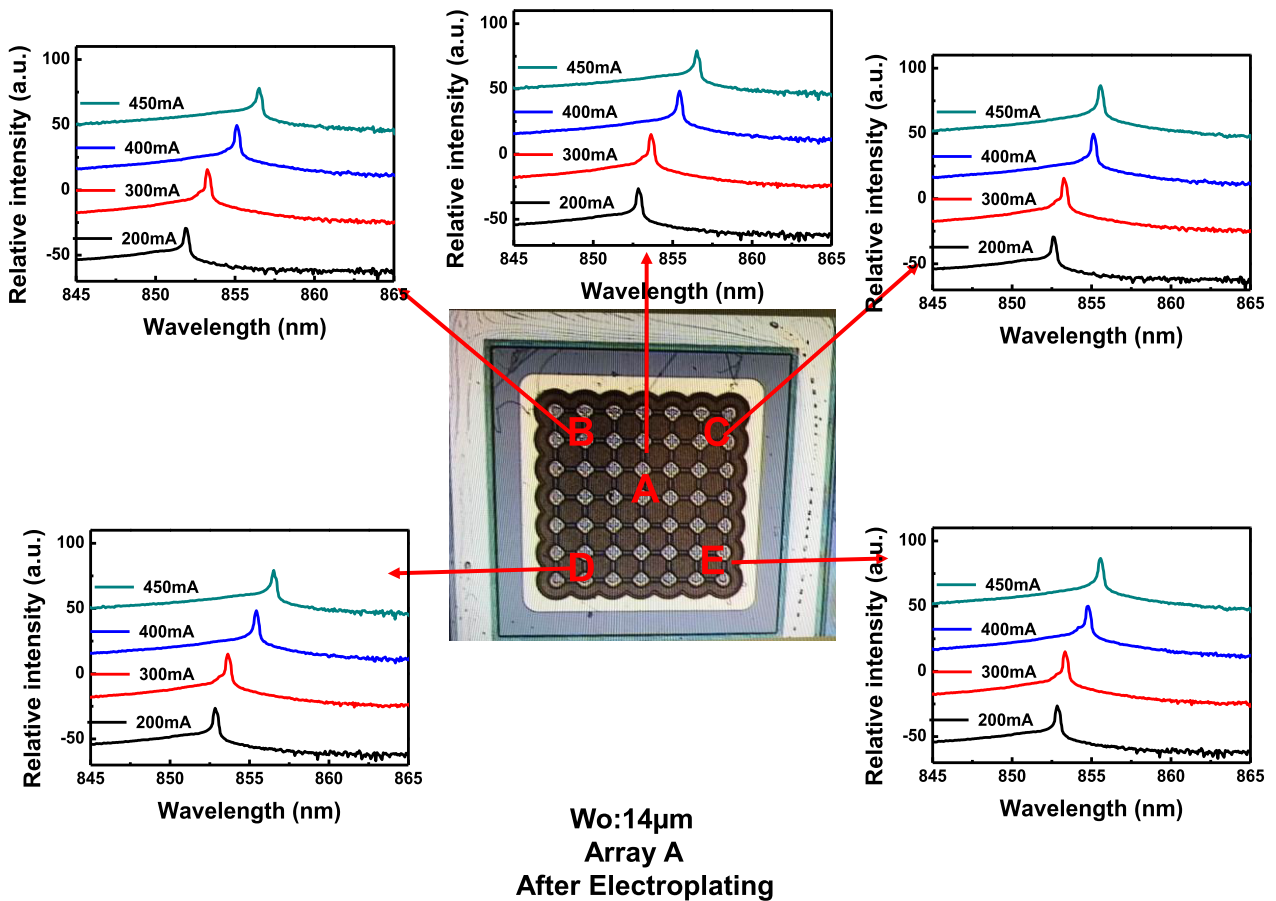


FIGURE 13. Measured bias dependent optical spectra of array A (W_0 : 14 μm) at different locations on the array under continuous wave (CW) operation after electroplating of the copper substrate.

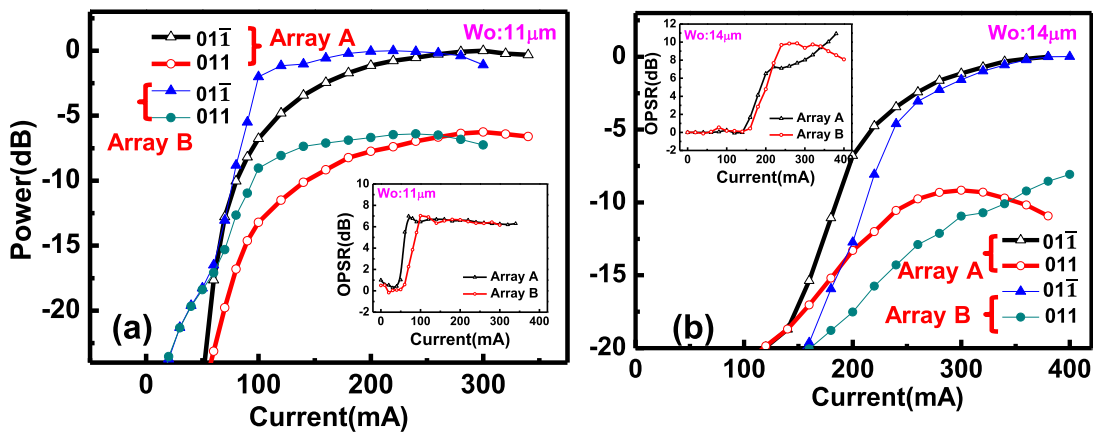


FIGURE 14. (a) Measured L-I curves of array A and array B at different orientations (0° : $\langle 011 \rangle$, 90° : $\langle 011 \bar{} \rangle$) with the polarizer and corresponding OPSR vs. bias current (inset) having oxide apertures of (a) W_0 : 11 μm and (b) W_0 : 14 μm .

(2 to 3 modes) and the applied external stress (from the electroplated copper substrate) is not strong enough to cause it to switch to highly SM performance with a highly single polarized output. Moreover, the output optical spectra of array B are already highly SM for both oxide aperture sizes

(W_0 : 11 and 14 μm) before the electroplating process is performed, as shown in Figure 8. The influence of this process on its output spectra and polarization states thus becomes less, as will be discussed later. Figures 14 (a) and (b) show the measured L-I curves for these two array orientations

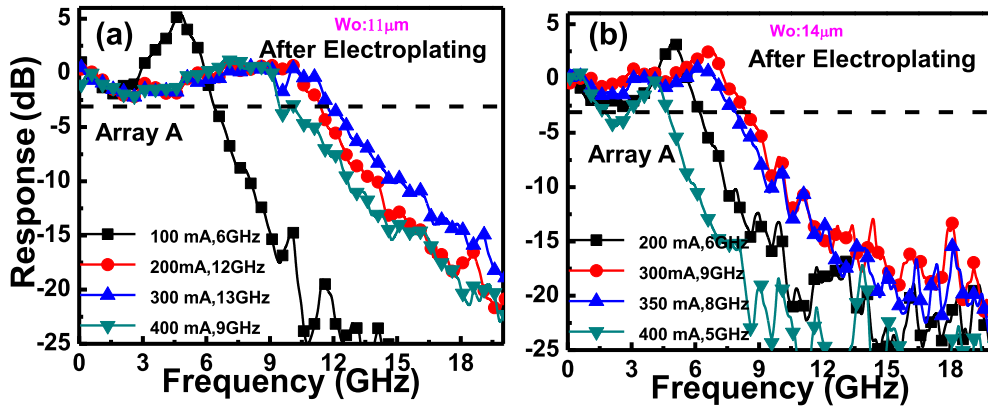


FIGURE 15. Measured bias dependent E-O frequency response of array A with W_o as (a) $11 \mu\text{m}$ and (b) $14 \mu\text{m}$ after performing the electroplating process.

(A and B) after electroplating with W_o equal to $11 \mu\text{m}$ and $14 \mu\text{m}$, respectively. The corresponding OPSR vs. bias current is also given in the inset. A rotational arm connected to a well-calibrated optical sensor head with a polarizer mounted on its window is adopted for measurement. The orientation of this polarizer is rotated during measurement to extract the output power component at different polarization states. We can clearly see that both arrays can maintain a stable polarization state output along $\langle 01\bar{1} \rangle$ but the OPSR of array A is larger than that of array B under a high bias current ($>300 \text{ mA}$) for the W_o equals $14 \mu\text{m}$ case. This may lead to a lower RIN and better eye-patterns performance under large signal modulation [29], as will be discussed later. The stable polarized output along the $\langle 01\bar{1} \rangle$ orientation of our array can be attributed to the growth of the epi-layer on the misoriented GaAs substrate [33] and the external stress induced by the electroplating of the copper substrate [27]. Under such external stress, the QSM performance ($W_o: 14 \mu\text{m}$) of array A switches to SM, as shown in Figure 13, due to the enhancement in selectivity of single polarized states, which usually leads to fundamental single-mode lasing [27]. On the other hand, with a smaller W_o of $11 \mu\text{m}$, the OPSR of both arrays (A and B) decreases from 10 to 6 dB. This degradation can be attributed to the output optical spectra still not being able to switch from QSM (or MM) to SM after the electroplating process, as discussed in Figure 13. Figures 15 (a) and (b) show the measured bias dependent E-O frequency responses of array A after electroplating for the different oxide aperture sizes of W_o : 11 and $14 \mu\text{m}$, respectively. Compared with the corresponding measurement results for array A before electroplating, as shown in Figure 10. We can clearly see that the device with a $14 \mu\text{m}$ W_o suffers a more significant SHB effect i.e., low-frequency roll-off, in its measured E-O frequency response after electroplating. Such a change simply reflects the significant variation in optical spectra and FFP, as discussed above. Nevertheless, the minor SHB induced low-frequency roll-off in array A after

electroplating leads to a diminishing in the resonant peak in the E-O response. This may lead to a lower RIN and an improvement in the quality of the eye patterns under large signal modulation. Figure 16 shows the measured 12.5 Gbit/sec eye patterns of arrays A and B (before/after electroplating), respectively. During measurement, a multi-mode fiber (MMF; OM3) with a ball lens tip is used to collect the light output from one of the single emitters in the array. The output of the MMF is then connected with a high-speed photo-receiver module (VI Systems3: R50-1300;), comprised of a p-i-n photodiode and limiting amplifier with a 3-dB optical-to-electrical (O-E) bandwidth of around 30 GHz. The O-E converted signal is then fed into a sampling scope to record and analyze the eye patterns. A 12.5 Gbit/s non-return-to-zero (NRZ) electrical signal with a pseudo-random binary sequence (PRBS) length of $2^{15}-1$ is generated using a pattern generator to drive the VCSELs. Both arrays (A and B) are tested under the optimized and same peak-to-peak driving voltage (0.9 V) to evaluate the quality of the eye patterns. Array A shows a better quality of eye patterns than array B, including less timing jitter, larger eye height/width, and a narrower far-field divergence angle, as specified in these figures. Furthermore, after electroplating, array A also shows an even more significant improvement in the quality of the eye patterns than array B. The superior dynamic performance of array A can be attributed to its extended passive waveguide (crisscross mesas) which can minimize the serious SHB effect and the serious low-frequency roll-off ($\sim 5 \text{ dB}$) induced in E-O responses, as illustrated in Figures 10 and 15. There is a slight enhancement of the SHB phenomenon in array A after electroplating due to the switching of its output optical spectra from QSM to SM, which pulls down the resonance in the E-O response as well as the RIN peak and thus improves the eye pattern quality. The non-obvious improvement in eye pattern quality of array B after electroplating can be attributed to the invariant SM optical spectra shown by array B before and after electroplating. Figures 17 (a) and (b) shows the measured frequency responses of RIN for array A

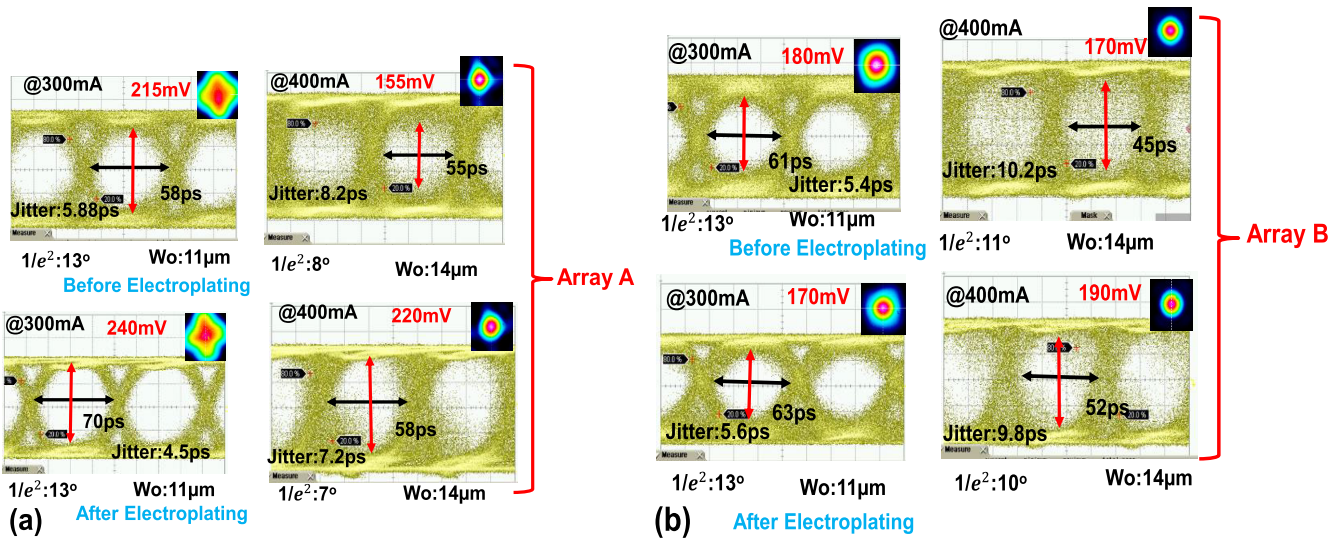


FIGURE 16. Measured 12.5 Gbit/sec eye patterns of (a) array A and (b) array B before and after the electroplating process.

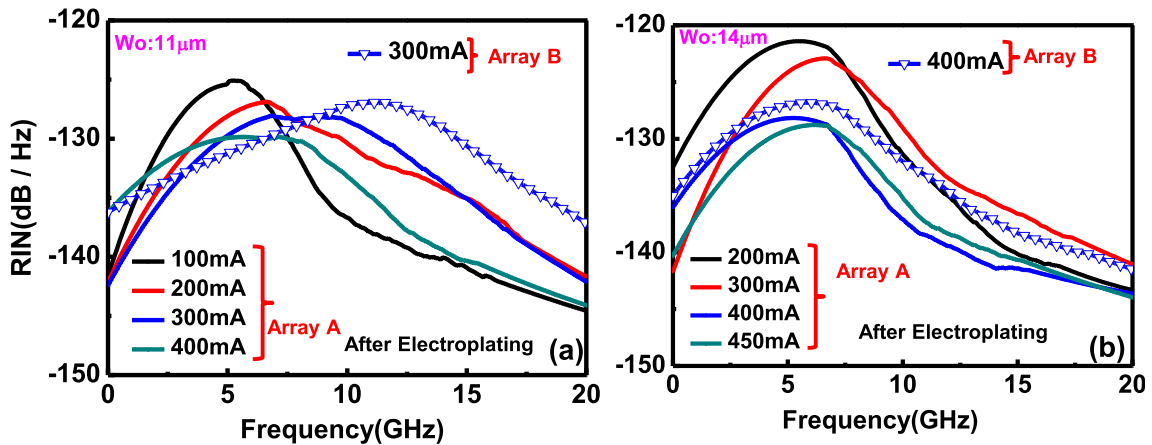


FIGURE 17. RIN frequency responses of array A and B after electroplating of the copper substrate with (a) W_o : 11 μm and (b) W_o : 14 μm .

(after electroplating) with W_o of 11 and 14 μm , respectively, under different bias currents.

The RIN of array B measured under a fixed bias current (300 or 400 mA), the same as that of array A, is also given in this figure for comparison. During our measurement, the thermal noise was carefully de-embedded. The shot noise can be neglected because it is too small under the photocurrent (~ 1 mA) typically used during measurement. For more detail about our RIN measurement setup please refer to [34]. We can clearly see that there is a gradual decrease in the peak of the RIN with the increase of bias current. In addition, the RIN peak of the array with a smaller oxide aperture (11 vs. 14 μm) is lower. These phenomena can be attributed to the minimization of the RIN by the increase of carrier/photon density as is usually observed in VCSELs [9], [34]. Moreover, the RIN peak exhibited by array A is comparatively lower than that exhibited by array B (~ 3 dB difference) under the same corresponding bias current. The improved RIN performance of array A can

be attributed to its larger OPSR and flatter E-O responses than those of array B, as illustrated in Figures 14 and 15. The lower RIN performance in turn leads to the better eye pattern quality. Overall, the demonstrated novel VCSEL array structure provides a breakthrough in the brightness of the output beam, RIN (< -130 dB/Hz), and improvement in the eye-pattern quality under large signal modulation.

IV. SUMMARY

In this work, we demonstrate a high-speed 850 nm VCSEL structure fabricated based on the Zn-diffusion technique with record high brightness output and a novel design for a VCSEL array capable of attaining a larger available power and overcoming the fundamental trade-off between the brightness, speed, and RIN of a single device with such a high-brightness performance. Using Zn-diffusion and the inclusion of oxide-relief apertures in the VCSEL units of the array will simultaneously relax the RC-limited bandwidth and improve the brightness performance of the

output beam. Furthermore, the effective optical volume (near field size) of each VCSEL unit can be increased by inserting passive waveguides to bridge the neighboring active VCSEL mesas, which in turn leads to narrowing of the far-field divergence angles, higher brightness, higher output power, and superior large signal modulation performance than those of the traditional VCSEL array without such waveguide connections. This enhancement of the static and dynamic performance can be attributed to the fact that the SHB effect has been greatly minimized due to the dilution of the photon density in the enlarged optical cavity. Moreover, the application of the additional electroplated copper substrate onto the demonstrated array leads to further improvements in the RIN, brightness, and eye-pattern quality under large signal modulation. These occur because the external stress induced by the integrated copper substrate results in highly SM, single polarized outputs (OPSR > 10 dB), and a minor SHB effect, acting to suppress the RIN peak and benefit the transmission performance. The demonstrated array can simultaneously achieve clear 12.5 Gbit/sec eye-opening, a $1/e^2$ far-field divergence angle as narrow as 7° , highly SM and single polarized outputs with a high maximum available CW output power of up to 90 mW. The demonstrated array structure opens new possibilities for the development of the next generation of optical wireless communication with a larger product of data rate and free space linking distance

REFERENCES

- [1] H. Kazemi, E. Sarbazi, M. D. Soltani, M. Safari, and H. Haas, "A Tb/s indoor optical wireless backhaul system using VCSEL arrays," in *Proc. IEEE 31st Annu. Int. Symp. Pers., Indoor Mobile Radio Commun.*, Sep. 2020, pp. 1–6.
- [2] M. Z. Chowdhury, M. T. Hossan, A. Islam, and Y. M. Jang, "A comparative survey of optical wireless technologies: Architectures and applications," *IEEE Access*, vol. 6, pp. 9819–9840, 2018.
- [3] P. Shubert, A. Cline, J. McNally, and R. Pierson, "System design of low SWaP optical terminals for free space optical communications," *Proc. SPIE*, vol. 10096, Feb. 2017, Art. no. 100960U.
- [4] D. Guilhot and P. Ribes-Pleguezuelo, "Laser technology in photonic applications for space," *Instruments*, vol. 3, no. 3, p. 50, Sep. 2019.
- [5] R. F. Carson, E. W. Taylor, A. H. Paxton, H. Schone, K. D. Choquette, H. Q. Hou, M. E. Warren, and K. L. Lear, "Surface-emitting laser technology and its application to the space radiation environment," *Proc. SPIE*, vol. 10288, Jul. 1997, Art. no. 1028806.
- [6] P. M. Goorjian, "Free-space optical communication for CubeSats in low lunar orbit (LLO)," *Proc. SPIE*, vol. 11272, Mar. 2020, Art. no. 1127214.
- [7] R. Safaisini, J. R. Joseph, and K. L. Lear, "Scalable high-CW-Power high-speed 980-nm VCSEL arrays," *IEEE J. Quantum Electron.*, vol. 46, no. 11, pp. 1590–1596, Nov. 2010.
- [8] N. Haghighi, P. Moser, and J. A. Lott, "Power, bandwidth, and efficiency of single VCSELs and small VCSEL arrays," *IEEE J. Sel. Topics Quantum Electron.*, vol. 25, no. 6, pp. 1–15, Dec. 2019.
- [9] D. M. Kuchta, J. Gamelin, J. D. Walker, J. Lin, K. Y. Lau, and J. S. Smith, "Relative intensity noise of vertical cavity surface emitting lasers," *Appl. Phys. Lett.*, vol. 62, pp. 1194–1196, Mar. 1993.
- [10] P. Westbergh, J. S. Gustavsson, B. Kögel, A. Haglund, and A. Larsson, "Impact of photon lifetime on high-speed VCSEL performance," *IEEE J. Sel. Topics Quantum Electron.*, vol. 17, no. 6, pp. 1603–1613, Nov. 2011.
- [11] J.-L. Yen, K.-L. Chi, J.-W. Jiang, Y.-J. Yang, and J.-W. Shi, "Single-mode vertical-cavity surface-emitting lasers array with Zn-diffusion aperture for high-power, single-spot, and narrow divergence angle performance," *IEEE J. Quantum Electron.*, vol. 50, no. 10, pp. 787–794, Aug. 2014.
- [12] Z. Khan, J.-C. Shih, R.-L. Chao, T.-L. Tsai, H.-C. Wang, G.-W. Fan, Y.-C. Lin, and J.-W. Shi, "High-brightness and high-speed vertical-cavity surface-emitting laser arrays," *Optica*, vol. 7, no. 4, pp. 267–275, Apr. 2020.
- [13] A. Haglund, J. S. Gustavsson, J. Vukusic, P. Modh, and A. Larsson, "Single fundamental-mode output power exceeding 6 mW from VCSELs with a shallow surface relief," *IEEE Photon. Technol. Lett.*, vol. 16, no. 2, pp. 368–370, Feb. 2004.
- [14] J.-W. Shi, C.-C. Chen, Y.-S. Wu, S.-H. Guol, and Y.-J. Yang, "High-power and high-speed Zn-diffusion single fundamental-mode vertical-cavity surface-emitting lasers at 850-nm wavelength," *IEEE Photon. Technol. Lett.*, vol. 20, no. 13, pp. 1121–1123, Jul. 6, 2008.
- [15] A. Furukawa, S. Sasaki, M. Hoshi, A. Matsuzono, K. Moritoh, and T. Baba, "High-power single-mode vertical-cavity surface-emitting lasers with triangular holey structure," *Appl. Phys. Lett.*, vol. 85, pp. 5161–5163, Nov. 2004.
- [16] N. N. Ledentsov, V. A. Shchukin, V. P. Kalosha, N. N. Ledentsov, Jr., J.-R. Kropp, M. Augustin, L. Chorchos, J. P. Turkiewicz, and J.-W. Shi, "Anti-waveguiding vertical-cavity surface-emitting laser at 850 nm: From concept to advances in high-speed data transmission," *Opt. Exp.*, vol. 26, no. 1, pp. 445–453, Jan. 2018.
- [17] J.-W. Shi, Z.-R. Wei, K.-L. Chi, J.-W. Jiang, J.-M. Wun, I.-C. Lu, J. Chen, and Y.-J. Yang, "Single-mode, high-speed, and high-power vertical-cavity surface-emitting lasers at 850 nm for short to medium reach (2 km) optical interconnects," *J. Lightw. Technol.*, vol. 31, no. 24, pp. 4037–4044, Dec. 10, 2013.
- [18] A. Haglund, J. S. Gustavsson, P. Modh, and A. Larsson, "Dynamic mode stability analysis of surface relief VCSELs under strong RF modulation," *IEEE Photon. Technol. Lett.*, vol. 17, no. 8, pp. 1602–1604, Aug. 25, 2005.
- [19] T. Grundl, P. Debernardi, M. Müller, C. Grasse, P. Ebert, K. Geiger, M. Ortsiefer, G. Bohm, R. Meyer, and M.-C. Amann, "Record single-mode, high-power VCSELs by inhibition of spatial hole burning," *IEEE J. Sel. Topics Quantum Electron.*, vol. 19, no. 4, Jul. 2013, Art. no. 1700913.
- [20] L. A. Coldren, S. W. Corzine, and M. L. Mašanović, *Diode Lasers and Photonic Integrated Circuits*, 2nd ed. Hoboken, NJ, USA: Wiley, 2012, ch. 5.
- [21] J.-W. Shi, L.-C. Yang, C.-C. Chen, Y.-S. Wu, S.-H. Guol, and Y.-J. Yang, "Minimization of damping in the electrooptic frequency response of high-speed Zn-diffusion single-mode vertical-cavity surface-emitting lasers," *IEEE Photon. Technol. Lett.*, vol. 19, no. 24, pp. 2057–2059, Dec. 4, 2007.
- [22] F. Koyama and X. Gu, "Beam steering, beam shaping, and intensity modulation based on VCSEL photonics," *IEEE J. Sel. Top. Quantum Electron.*, vol. 19, no. 4, Jul./Aug. 2013, Art. no. 1701510.
- [23] N. Haghighi, P. Moser, M. Zorn, and J. A. Lott, "19-element vertical cavity surface emitting laser arrays with inter-vertical cavity surface emitting laser ridge connectors," *J. Phys., Photon.*, vol. 2, no. 4, Oct. 2020, Art. no. 04LT01.
- [24] J.-C. Shih, Z. Khan, Y.-H. Chang, and J.-W. Shi, "High-brightness VCSEL arrays with inter-mesa waveguides for the enhancement of efficiency and high-speed data transmission," *IEEE J. Sel. Topics Quantum Electron.*, vol. 28, no. 1, pp. 1–11, Jan. 2022.
- [25] J.-L. Yen, X.-N. Chen, K.-L. Chi, J. Chen, and J.-W. Shi, "850 nm vertical-cavity surface-emitting laser arrays with enhanced high-speed transmission performance over a standard multimode fiber," *J. Lightw. Technol.*, vol. 35, no. 15, pp. 3242–3249, Mar. 1, 2017.
- [26] C.-L. Cheng, N. Ledentsov, Z. Khan, J.-L. Yen, N. N. Ledentsov, and J.-W. Shi, "Ultrafast Zn-diffusion and oxide-relief 940 nm vertical-cavity surface-emitting lasers under high-temperature operation," *IEEE J. Sel. Topics Quantum Electron.*, vol. 25, no. 6, pp. 1–7, Dec. 2019.
- [27] J.-W. Shi, Z. Khan, R.-H. Horng, H.-Y. Yeh, C.-K. Huang, C.-Y. Liu, J.-C. Shih, Y.-H. Chang, J.-L. Yen, and J.-K. Sheu, "High-power and single-mode VCSEL arrays with single-polarized outputs by using package-induced tensile strain," *Opt. Lett.*, vol. 45, no. 17, pp. 4839–4842, Aug. 2020.
- [28] D. V. Kuksenkov, H. Temkin, and S. Swirhun, "Polarization instability and relative intensity noise in vertical-cavity surface-emitting lasers," *Appl. Phys. Lett.*, vol. 67, no. 15, pp. 2141–2143, Oct. 1995.
- [29] T. Yoshikawa, T. Kawakami, H. Saito, H. Kosaka, M. Kajita, K. Kurihara, Y. Sugimoto, and K. Kasahara, "Polarization-controlled single-mode VCSEL," *IEEE J. Quantum Electron.*, vol. 34, no. 6, pp. 1009–1015, Jun. 1998.
- [30] M. Yoshida, M. De Zoysa, K. Ishizaki, Y. Tanaka, M. Kawasaki, R. Hatsuda, B. Song, J. Gellera, and S. Noda, "Double-lattice photonic-crystal resonators enabling high-brightness semiconductor lasers with symmetric narrow-divergence beams," *Nature Mater.*, vol. 18, pp. 121–128, Feb. 2019.

- [31] E. Haglund, M. Jahed, S. J. Gustavsson, A. Larsson, J. Goyvaerts, R. Baets, G. Roelkens, M. Rensing, and P. O'Brien, "High-power single transverse and polarization mode VCSEL for silicon photonics integration," *Opt. Exp.*, vol. 27, no. 13, pp. 18892–18899, Jun. 2019.
- [32] P.-C. Pan, D. Nag, Z. Khan, C.-J. Chen, J.-W. Shi, A. Laha, and R.-H. Horng, "Effect of thermal management on the performance of VCSELs," *IEEE Trans. Electron Devices*, vol. 67, no. 9, pp. 3736–3739, Sep. 2020.
- [33] Y.-G. Ju, Y.-H. Lee, H.-K. Shin, and I. Kim, "Strong polarization selectivity in 780-nm vertical-cavity surface-emitting lasers grown on misoriented substrates," *Appl. Phys. Lett.*, vol. 71, no. 6, pp. 741–743, Jun. 1997.
- [34] S.-E. Hashemi, "Relative intensity noise (RIN) in high-speed VCSELs for short reach communication," M.S. thesis, Dept. Microtechnol. Nanosci., Chalmers Univ. Technol., Gothenburg, Sweden, 2012.



ZUHAIB KHAN was born in Uttar Pradesh, India, in 1992. He received the degree from the Department of Electronics and Communication Engineering, Jamia Millia Islamia, New Delhi, India. He is currently pursuing the Ph.D. degree with the Department of Electrical Engineering, National Central University, Taiwan. His current research interests include high-speed, high-power VCSELs for application to optical interconnects, 3D-sensing, autonomous LIDAR, and time of flight.



YUNG-HAO CHANG was born in Tainan, Taiwan, in November 1996. He received the degree from the Department of Electrical Engineering, Yuan Ze University, Taoyuan, Taiwan. He is currently pursuing the master's degree with the Department of Electrical Engineering, National Central University, Taoyuan. His current research interests include high-speed and high-power VCSELs.



TE-LIEH PAN was born in Keelung, Taiwan, in August 1969. He received the master's degree in business administration from the Jinwen University of Science and Technology, New Taipei, Taiwan. He is currently pursuing the degree with the Graduate Institute of Electro-Optical Engineering, Chang Gung University, Taoyuan, Taiwan. He is currently the Vice President with AboCom System Inc., responsible for the research and development and the production of VCSELs and holds three VCSEL-related patents.



YAUNG-CHENG ZHAO was born in New Taipei, Taiwan, in October 1996. He received the bachelor's degree from the Department of Electrical Engineering, National University of Kaohsiung, Kaohsiung, Taiwan. He is currently pursuing the master's degree with the Department of Electrical Engineering, National Central University, Taoyuan, Taiwan. His current research interests include high-speed and high-power VCSELs.

YEN-YU HUANG, photograph and biography not available at the time of publication.

CHIA-HUNG LEE, photograph and biography not available at the time of publication.

JUI-SHENG CHANG, photograph and biography not available at the time of publication.



CHENG-YI LIU was born in Hualien, Taiwan. He received the Ph.D. degree in materials science and engineering from the University of California, Los Angeles, USA, in 2000. He is currently a Professor with the Department of Chemical and Materials Engineering and the Director of the Optical Sciences Center, National Central University, Taoyuan, Taiwan. His research interests include optoelectronic, micro-electro-mechanical systems, multilayer metallization process in semiconductor, and metal nanowire.



CHENG-YUAN LEE was born in Taoyuan, Taiwan, in May 1992. He received the degree from the Institute of Optoelectronic Engineering, Chang Gung University, where he is currently pursuing the Ph.D. degree in electronic engineering. His current research interests include high-speed, high-power VCSELs, long-wavelength VCSEL, and EEL.



CHAO-YI FANG was born in Tainan, Taiwan, in November 1969. He received the B.S. degree in chemistry from National Tsing-Hua University, Hsinchu, Taiwan, and the Ph.D. degree in material science and engineering from National Chiao Tung University, Hsinchu, in 2004, with dissertation entitled "Material Characterizations and Process Development of W_Nx T-gate AlGaIn/GaN High Electron Mobility Transistor for High Temperature Applications." He has been involved in semiconductor industry, since 1991, including Si epitaxy, GaN base epitaxy and devices, and GaAs base epitaxy and devices. So far, he holds 23 patents in his professional field.



JIN-WEI SHI (Senior Member, IEEE) was born in Kaohsiung, Taiwan, in January 1976. He received the B.S. degree in electrical engineering from National Taiwan University, Taipei, Taiwan, in 1998, and the Ph.D. degree from the Graduate Institute of Electro-Optical Engineering, National Taiwan University, in 2002. He was a Visiting Scholar with the University of California at Santa Barbara (UCSB), CA, USA, from 2000 to 2001. From 2002 to 2003, he held a postdoctoral position with the Electronic Research and Service Organization, Industrial Technology Research Institute (ITRI). In 2003, he joined the Department of Electrical Engineering, National Central University, Taoyuan, Taiwan, where he is currently a Professor. In 2011, he again joined the ECE Department, UCSB, as a Visiting Scholar. He has authored or coauthored more than 140 journal articles, 160 conference papers, and hold 20 patents. His current research interests include ultrahigh speed/power optoelectronic devices, such as photodetectors, electro-absorption modulators, submillimeter wave photonic transmitters, and semiconductor lasers. He was an Invited Speaker at the 2002 IEEE LEOS, the 2005 SPIE Optics East, the 2007 Asia-Pacific Microwave Photonic Conference (AP-MWP), the 2008 Asia Optical Fiber Communication and Optoelectronic Exposition and Conference (AOE), the 2011 Optical Fiber Communication (OFC), and the 2012 IEEE Photonic Conference (IPC). He served on the Technical Program Committees for the OFC 2009–2011, 2012 SSDM, 2012 MWP, and 2013 Asia-Pacific CLEO. In 2007, he was a recipient of the Excellent Young Researcher Award from the Association of Chinese IEEE and the Da-You Wu Memorial Award, in 2010.

...